One-Pot Production of 1,5-Pentanediol from Furfural Through Tailored Hydrotalcite-Based Catalysts

A. Barranca[1] · I. Gandarias[1] · P. L. Arias[1] · I. Agirrezabal-Telleria[1]

Abstract

The one-pot production of a relevant chemical such as 1,5-pentanediol (1,5-PDO) from sustainable sources (furfural) is a key reaction to compete with existing fossil sources. This work provides new evidence on the influence of the starting reagent, the features of layered double hydrotalcite (LDH)-derived catalysts in the form of mixed metal oxides (MMO) and of reaction conditions on the productivity of 1,5-PDO under batch conditions. Unlike reported studies, these results suggest the direct pathway through furfuryl alcohol intermediates, allowing the one-pot production from furfural at lower temperature than analogous systems. Productivity is maximized when Co^{2+} species partially substitute Mg^{2+} species in parent LDH, yielding promising pentanediol yields under mild reaction conditions. MMOs containing Co^{2+} sites show marked differences compared to analogous bivalent metals, which is here attributed to the position in which reaction intermediates such as furfuryl alcohol are adsorbed onto surface specie. This is consistent with characterized surface species by XRD, temperature programmed reduction under H_2, and chemisorption experiments using CO or CO_2 as probe molecules, indicative of a proper balance between metal and basic sites onto MMOs. The reported data aim to provide new reaction evidence to contribute into the search of sustainable 1,5-PDO sources.

Graphical Abstract

Tuning metal functions onto hydrotalcites to produce 1,5-pentanediol from furfural
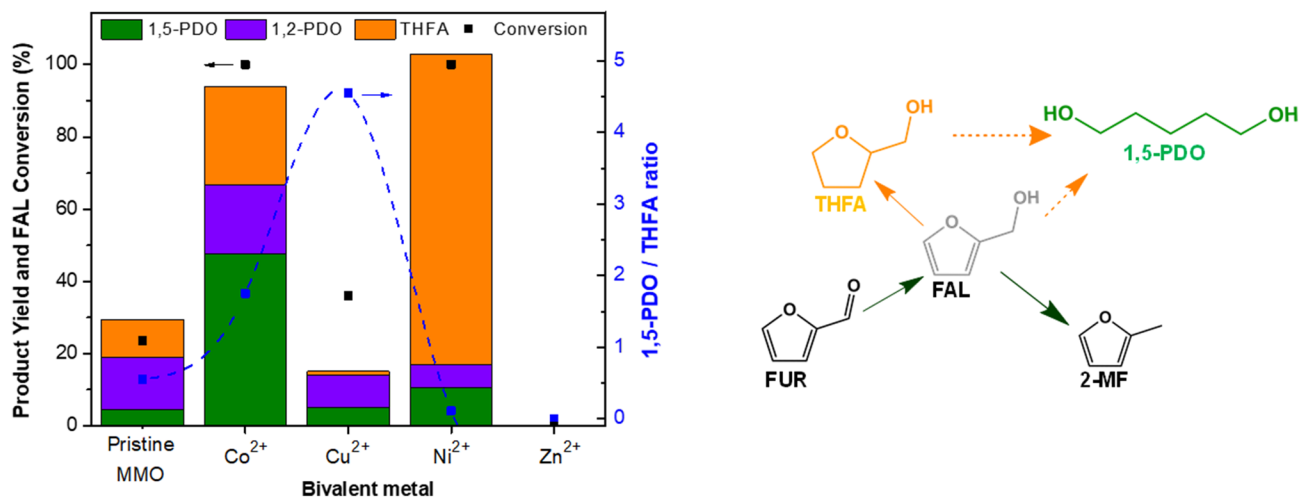
✉ I. Agirrezabal-Telleria
 iker.aguirrezabal@ehu.eus

Extended author information available on the last page of the article

Abbreviations

FUR	Furfural
FAL	Furfuryl alcohol

THFA   Tetrahydrofurfuryl alcohol
1,5-PDO   1,5-Pentanediol
1,2-PDO   1,2-Pentanediol
2-MF   2-Methylfuran
MMO   Mixed metal oxide
LDH   Layered double hydrotalcite
TPR   Temperature-programme reduction
XRD   X-ray diffraction

1 Introduction

1,5-Pentanediol (1,5-PDO) is a compound of notable interest in the polymer industry, as it allows the manufacture of polyesters and polyurethanes via a more economic and sustainable pathway than analogues, such as 1,4-butanediol and 1,6-hexanediol [1, 2]. In this context, furfural (FUR) is a key platform bio-chemical to search alternative 1,5-PDO production routes [3–7]. 1,5-PDO can be formed via two main routes from FUR derivatives: (i) ring-opening hydrogenolysis of tetrahydrofurfuryl alcohol (THFA) via furfuryl alcohol (FAL) hydrogenation, or (ii) the direct ring-opening hydrogenolysis of FAL. The direct route presents several advantages, especially as it enables the one-step 1,5-PDO production from FUR using less reaction and intermediate purification stages. In addition, tailored catalysts avoid the possible presence of side-products from THFA affecting downstream 1,5-PDO purity.

Among the heterogeneous catalysts of interest, hydrotalcites in the form of Layered Double Hydroxides (LDH) offer numerous advantages for such purpose. LDH consist of positively charged laminar layers (generally Mg^{2+} and another trivalent metal) [8] and contain H_2O and compensation anions such as OH^-, CO_3^{2-} or NO_3^- [9, 10]. For Al^{3+}, LDH are named hydrotalcites [11]. They present multiple structural versatility by substituting cationic charge and great adsorption capacity after converting LDHs into mixed metal oxides (MMO) via calcination. The nature of the M^{2+}/M^{3+} ions allows tuning their stability and catalytic performance [12] in reactions such as aldol condensation, transesterification or alkylation.

The use of these catalytic systems in the hydrogenation of FUR derivatives into 1,5-PDO is still under development [3–6, 13–17]. The reported systems often use THFA as starting reagent. Even when 1,5-PDO yields are over 60%, such reagents limit their direct implementation within the FUR platform. Among LDH-based supports, Cu and Ni species form undesired products [FAL and cyclopentanones (CPOs)] [18] and thus lead to 1,5-PDO yields at ≤ 30% [19–21]. Remarkable yields were obtained when Co species catalyze such reactions. Noble metals such as Rh contribute to remarkable FUR hydrogenation/hydrogenolysis activity, but

predominantly form 1,2-PDO (85%) compared to 1,5-PDO. [22]

This work shows new evidences on the role of the nature of bivalent metals (Co^{2+}, Cu^{2+}, Zn^{2+}, Ni^{2+}), the effects of the type of reactant, the presence of Pt as hydrogenating site and reaction conditions on the direct 1,5-PDO pathway from FUR. Mg^{2+} species were partially substituted by bivalent metals in parent hydrotalcite structures, and after being transformed into MMO, these were tested under batch conditions. Surface Pt sites served to activate H_2. The results indicate the predominance for the direct hydrogenolysis and ring-opening of FAL intermediates from FUR when using Co^{2+}-based materials. These results outstand compared to those obtained using the rest of the studied metals, especially as 1,5-PDO is effectively produced in one-pot at lower reaction temperatures [23]. Thus, this work is expected to contribute to pave the way towards alternative and feasible pathways to produce sustainable polymers from 1,5-PDO.

2 Experimental Section

The MMO materials were prepared by titrating the corresponding aqueous precursors of M^{2+} nitrates and NaOH into a solution of sodium carbonate in a round flask with agitation. The molar ratio of trivalent (Al^{3+}) and divalent metals (M^{2+}) was preserved 1:4 even when Mg^{2+} was partially substituted by M^{2+} (Co^{2+}, Cu^{2+}, Zn^{2+} or Ni^{2+}) within the parent hydrotalcite. The CO_3^-:Al^{3+} ratio remained 1:2. The as-obtained MMOs showed the $Mg_{0.6}M^{2+}_{0.2}Al_{0.2}$ atomic composition. The synthesis pH was preserved at 9 for 1 h at room temperature under stirring. The water in the solution was evaporated at 333 K overnight. The as-obtained solid was contacted with abundant water in a funnel to ensure a filtrate pH of 7. This solid was dried in a static oven at 378 K in air overnight and treated under air flow at 773 K for 3 h to turn into MMO structures. Pt was introduced, at different mass contents, using two procedures: (i) impregnated by contacting the MMO with an aqueous Pt solution of the desired concentration for 1 h at room temperature; (ii) co-impregnated by including the Pt precursor in the initial aqueous solution with the other M^{2+} precursors. The as-obtained solids were filtered, contacted with water and dried as explained earlier. These were later treated under air flow at 623 K and subsequently under 5% H_2/He flow for 1 h at 623 K. The materials containing co-impregnated Pt are included within the MMO nomenclature at the given molar ratio, and the materials after sequential impregnation are shown as xPt@, where x refers to the Pt mass content.

XRD measurements were carried out in an automatic diffractometer (Philips X'pert PRO) at 40 kV and 40 mA, secondary monochromatic Cu-Kα radiation (λ = 1.5418 Å) and PIXcel solid state detector. Data were collected from

40° to 55° 2 theta. H_2-TPR profiles were obtained using 50 mL min^{-1} of 5% H_2/He in an Autochem II (*Micromeritics*) equipped with a TCD detector. Samples were pretreated at 773 K under Ar atmosphere. The CO chemisorption experiments of as-reduced catalysts were carried out at 308 K using 50 mL min^{-1} of He and pulses of CO/He (0.01788 cm^3, 5% CO/He). CO_2 desorption experiments were performed after adsorbing CO_2 at 413 K and treatment in He up to 773 K. N_2-physisorption experiments were performed at 77 K using an Autosorb 1C-TCD unit (*Quantachrome*).

Activity tests were carried out in 50 mL stainless steel autoclaves using 10 mL of 2-propanol as solvent and reactants (1 g per g of catalyst) such as FUR (99.0%, *Sigma Aldrich*), FAL (98.0%, *Sigma Aldrich*) or THFA (99.0%, *Sigma Aldrich*). Iso-octane was used as internal standard for GC analysis. The reactor was purged with H_2 (99.9%, *Air Liquide*) and pressurized at 3.0 MPa in H_2 for catalysis. The solution was stirred at 500 rpm and the temperature controlled at 423 K by means of a hot plate. The reaction was stopped after 4 h by controlled cooling. Liquid products were analyzed in an *Agilent* 7890 gas-chromatograph with a DB-1 column (60 m × 530 μm × 5 μm) and a FID detector.

3 Results and Discussion

Figure 1A shows the X-ray diffraction patterns of the parent (bare) hydrotalcite and of the calcined materials modified with bivalent metals (Co^{2+}, Cu^{2+}, Ni^{2+}, Zn^{2+}). The parent material shows a typical spectrum corresponding to the $Mg_6Al_2(OH)_{18}4.5(H_2O)$ structure, indicating the tight Al–Mg interactions leading to double layered hydrotalcite structures. After calcination, all modified materials show the presence of MgO, confirming that developed synthesis and calcination protocols convert parent LDH into a mixture of metal oxides (MMO). All M^{2+}-containing MMOs present higher surface areas as well as more accessible pores than the pristine MMO, increasing pore size from 3 to 6–7 nm (Table 1). The partial substitution of Mg^{2+} by M^{2+} did not significantly modified the density of basic centers of the resulting MMO, as obtained via the desorption of chemisorbed CO_2. FAL hydrogenolysis is preceded by adsorption onto basic centers and M^{2+}, and thus the similar basic site density among all materials allows to rigorously evaluate the contribution of M^{2+} in catalysis. Catalyst surfaces preserve accessible basic centers, especially when H_2 dissociation species (Pt) are placed in stepwise impregnation methods, enabling the targeted hydrogenolysis catalytic steps, as shown later. Such surface speciation is also reflected in the consumption of H_2 as a function temperature (Fig. 1B). The pristine MMO contains strong Mg–Al bonds minimizing any H_2 consumption. Such interaction is not altered when
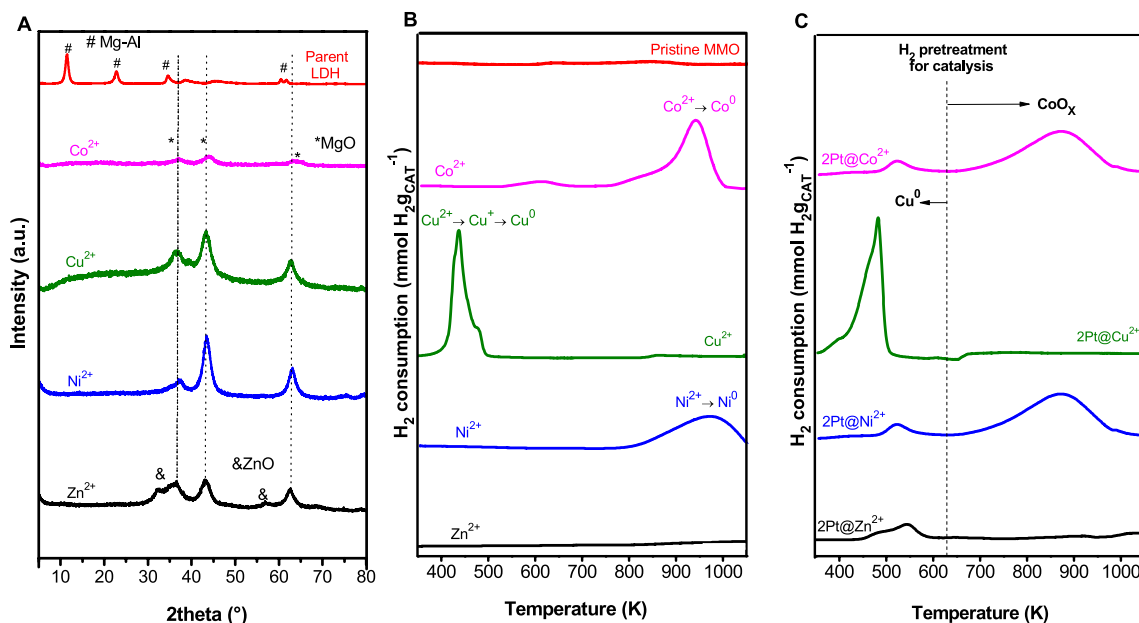

Fig. 1 A XRD patterns of parent LDH and MMOs containing bivalent metals; **B** H_2 consumption profiles for pristine MMO and for MMOs modified with different bivalent metals as a function of temperature; **C** H_2 consumption for modified MMOs impregnated with Pt as a function of temperature

Table 1 Characterization data on Pt-containing MMOs

Catalyst	Adsorbed CO (mmol CO g^{-1})	Pt dispersion* (%)	Crystal size (nm)	Adsorbed CO_2 (mmol CO_2 g^{-1})[a]	Density of basic centers (µmol CO_2 m^{-2})	BET surface area (m^2 g^{-1})	Pore size (nm)
2Pt@PristineMMO	0.020	20.1	4.7	0.14	0.93	151	3.63
2Pt@Co^{2+}	0.020	25.7	3.9	0.18	0.98	183	7.10
2Pt@Cu^{2+}	0.020	19.7	5.1	0.15	0.77	194	6.16
2Pt@Ni^{2+}	0.020	22.0	4.6	0.12	0.65	184	6.17
2Pt@Zn^{2+}	0.003	3.7	27.3	0.16	0.77	208	6.14
1Pt@Co^{2+}	0.010	26.7	3.8	_[a]	_[a]	_[a]	_[a]
4Pt@Co^{2+}	0.040	19.3	5.2	_[a]	_[a]	_[a]	_[a]

*Pt dispersion measured assuming stoichiometric CO adsorption onto Pt sites

[a]Not measured

Zn^{2+} is introduced, indicating the strong Zn affinity to O species [24]. The rest of MMOs, however, show marked H_2 consumption. The reduction of Cu^{2+}-derived oxides occurs at much lower temperatures (400–480 K) than for Co^{2+} or Ni^{2+} (800–1000 K). The smaller temperature shoulder for Cu^{2+} (400 K) corresponds to small and well-dispersed Cu clusters, whilst larger clusters require slightly higher temperatures [25, 26]. Such reduction may even take place in two reduction steps, with Cu^+ intermediates. Both Co^{2+}- and Ni^{2+}-oxide species are predominantly reduced above 900 K, corresponding to the presence of bivalent metals. These temperatures seem high for NiO, as compared to bulk NiO species (reduced at 600 K), indicating that the presence of MgO may stabilize NiO sites and thus limit their reducibility at low temperature [27].

Figure 1C shows the H_2-TPR profiles of the materials containing 2 wt% impregnated Pt. All 2Pt@M^{2+} materials nearly preserve the reduction profiles corresponding to bivalent metals and show an additional reduction peak at nearly 500 K. The Pt reduction may proceed through H_2 dissociation, and spillover phenomena may contribute into Co^{2+} and Ni^{2+} reduction at lower temperatures than in Pt absence (Fig. 1B). These H_2 consumption profiles served to adjust the catalyst pre-treatment in H_2 to 623 K and ensure

that Pt sites are reduced prior to catalyst testing. In the case of Cu^{2+} species, these are also reduced to Cu^0 at 623 K in H_2. The presence of surface Pt on MMOs is also confirmed by evaluating the Pt dispersion after CO adsorption (Table 1). Among the materials containing impregnated Pt, all materials except for 2Pt@Zn^{2+} show Pt dispersion of 20–25%, consistent with porous structures and accessible Pt sites. The amount of adsorbed CO is very similar for such materials, indicative of the presence of similar Pt species irrespective of the MMO nature. The amount of adsorbed CO is also nearly proportional to Pt content at 1–4 wt% on xPt@Co^{2+} samples (Table 1), but the Pt dispersion slightly decreases with Pt content. Even when H_2-TPR profile for co-impregnated materials are analogous to sequentially impregnated materials, the dispersion data are not evident for 2Pt@Zn^{2+} (3.7%) or Co^{2+}-based MMO after Pt co-impregnation (2.7%), mainly due to less accessible and larger Pt crystals originated from strong Pt and MMO interactions in the bulk phase, restricting the availability of dissociated H_2 on Pt sites intended for FAL hydrogenolysis, as discussed later.

Figure 2A shows the furfuryl alcohol (FAL) hydrogenolysis activity for 2Pt@M^{2+} materials and for 2Pt@PristineMMO under batch conditions at 423 K. The catalysts tested under these reaction conditions (2-propanol as

Fig. 2 **A** FAL hydrogenation conversion and product yields (left axis) and 1,5-PDO/THFA molar ratio (right axis) for 2Pt@pristineMMO or 2Pt@M^{2+} at 423 K, 30 bar H_2 and 4 h of reaction; **B** mechanism of FAL adsorption onto CoO_X or Cu^0-containing MMOs
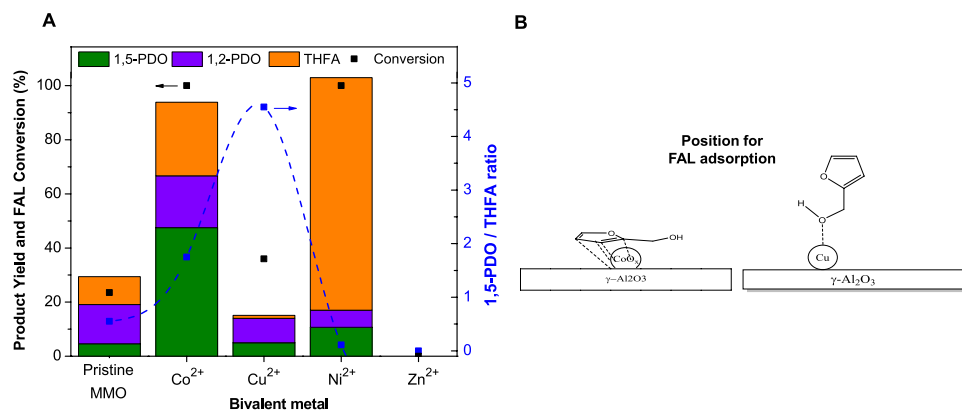
solvent) have a negligible contribution from water, and thus CPO is not detected as undesired product. The poor activity for 2Pt@PristineMMO may be attributed to: (i) the adsorption configuration of FUR or FAL molecules over Mg^{2+} species, which is inhibited due to the strong basic nature of Mg^{2+}. The adsorption may be favored at optimal strength (and not number) of basic centers, mostly favorable when Mg^{2+} species are partially substituted by Cu^{2+} or Co^{2+}; (ii) MMOs containing bivalent metals other than Mg^{2+} show much larger pore size distributions, with an increase from 3.6 to about 6–7 nm (Table 1). Such drastic change may affect the diffusion of bulky FUR or FAL under liquid solutions, limiting their catalytic turnover for 2Pt@PristineMMO. It is worth noting that bivalent metals such as Co^{2+}, Ni^{2+}, Zn^{2+} are used in their oxidized form prior to catalysis, except for Cu^0 (based on H_2-TPR in Fig. 1C). The poor dispersion of impregnated Pt^0 on 2Pt@Zn^{2+} is also reflected on its lack of catalytic activity during FAL hydrogenation (Fig. 2A). Such lack of activity may be attributed to the poisoning effect of Zn^{2+} species when titrating oxide materials with Pt, yielding very poor Pt dispersion and hydrogenolysis activity. REF Both Co^{2+} and Ni^{2+} show marked FAL conversion products, whereas the pristine MMO or Cu^0 species show much lower FAL hydrogenolysis activity. These data are consistent with the configuration angle of adsorbed FAL molecules on M^{2+} oxides, analogous to those observed for FUR [28, 29]. The overlapping of 3d orbitals on Cu^0 and the oxygen anti-bonding orbital on the furanic molecule of FAL lead to repulsive forces, yielding FAL molecules oriented in perpendicular manner and thus weakly interacting (Fig. 2B). On the contrary, CoO_X species allow a horizontal FAL surface configuration and thus enable the furanic C−O bond hydrogenolysis. This configuration may also be valid for 2Pt@Ni^{2+}, but its higher hydrogenating capacity predominantly leads to the full saturation of the furanic molecule into THFA [30]. The absence of products such as 2-methylfuran in all catalysts is consistent with the basic nature of MMOs, as acid sites are required for C−OH bond hydrogenolysis in FAL. In addition, the higher Pt dispersion and smaller crystal size for Co^{2+} MMOs favors the H_2 dissociation to proceed with hydrogenolysis reactions, yielding higher 1,5-PDO yields than Cu^{2+}. It is worth noting that conversion values for Co^{2+} and Ni^{2+} are nearly 100%, which may complicate an entirely correct understanding of the intrinsic kinetic activity of each specie. However, Fig. 2A clearly highlights the intended differences in 1,5-PDO yield in each Pt-containing MMO. In addition, C-balance (defined as number of detected C-atoms in products with respect to converted C atoms in FAL) is 90–105% in all cases, indicative of the presence of some products that were not identified and thus quantified after reaction.

As a remarkable result, the 2Pt@Co^{2+} catalyst shows a FAL hydrogenolysis yield of nearly 70% to pentanediols, with 1,5-PDO yield of 47% and a productivity of 1.2 $mol_{1,5\text{-PDO}}kg_{cat}^{-1}$ h^{-1}. These results outstand at lower reaction temperature compared to reported Pt-based hydrotalcites, especially, as FUR reactant, as shown later, obtains very similar yields [23]. In addition, it is worth noting that the 1,5-PDO yield for Co^{2+}-based MMOs synthesized after Pt co-impregnation is $< 1\%$, indicative of the relevance that Pt species, made only accessible via sequential impregnation (Fig. 2B), have in the H_2 activation for measured hydrogenolysis yields. [31, 32]

The literature shows a recurrent controversy on relevant reaction pathways towards 1,5-PDO from FUR. It is worth noting that the catalytic FUR hydrogenation into FAL is faster than the subsequent steps. Both reactants are here used to rigorously study the intended hydrogenolysis pathways on MMOs. We provide new evidences on the hydrogenation activity for Co^{2+} and Cu^{2+}-based MMOs using FUR, FAL or THFA as reactants (Fig. 3). Unlike many reported catalysts, Co^{2+} and Cu^{2+} species on such MMOs do not enable the hydrogenolysis of C−O bonds on THFA, leading to undetectable 1,5-PDO formation rates. The nearly complete FUR conversion for both active species reflects the rapid hydrogenation into the primary product (FAL), as depicted in the reaction network in Fig. 4. The 2Pt@Cu^{2+} catalyst, however, proceeds into further hydrogenolysis steps, forming 1,5-PDO as major product. Indeed, 1,5-PDO yields are identical when FUR or FAL are used as reactants (Fig. 3). These data indicate the prevalence of Co^{2+}-based MMOs to form 1,5-PDO via the direct ring-opening hydrogenolysis of FAL as intermediate, enabling the one-pot/step FUR to 1,5-PDO pathway at high catalytic yields. Figure 3B confirms the limited FAL hydrogenolysis activity on 2Pt@Cu^{2+}, irrespective of when FAL is formed from FUR or is used as reactant.

The 1,5-PDO formation rate is here optimized in terms of impregnated Pt^0 content and catalysis temperature for Co^{2+}-based MMOs. Figure 5 shows that both FAL conversion and 1,5-PDO yields increase with Pt^0 content. In the absence of Pt and Co^{2+}-derived MMOs, no reaction product was detected. 1,5-PDO yield reaches a maximum at 47% for the 2Pt@Co^{2+} at nearly complete FAL conversion. The 1,5-PDO/THFA ratio in Fig. 5 shows that higher Pt^0 contents favor THFA formation, indicative that the enhanced H_2 dissociation rate on Pt^0 sites [33] preferentially leads to furanic ring hydrogenation. The nearly complete FAL conversion above 2 wt% Pt indicates that surface basic sites, relevant for adsorbing FAL molecules through OH groups, are available even at the higher Pt contents. This is consistent with the nearly 20% Pt dispersion on 4Pt@Co^{2+} (Table 1), indicative of the minor formation of larger Pt clusters. The optimal reaction temperature is also independent of Pt content above 2 wt%. Higher temperatures favor the hydrogenolysis into 1,2-PDO over 1,5-PDO, suggesting that mild conditions at

Fig. 3 **A** Conversion and product yields (left axis) and 1,5-PDO/THFA molar ratio (right axis) for $2Pt@Co^{2+}$ at 423 K, 30 bar H_2 and 4 h of reaction as a function of type of reactant (FUR, FAL, THFA); **B** conversion and product yields (left axis) and 1,5-PDO/THFA molar ratio for $2Pt@Cu^{2+}$ at 423 K, 30 bar H_2 and 4 h of reaction as a function of type of reactant (FUR, FAL, THFA)
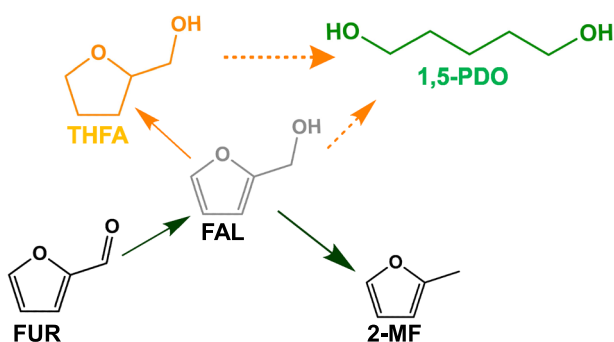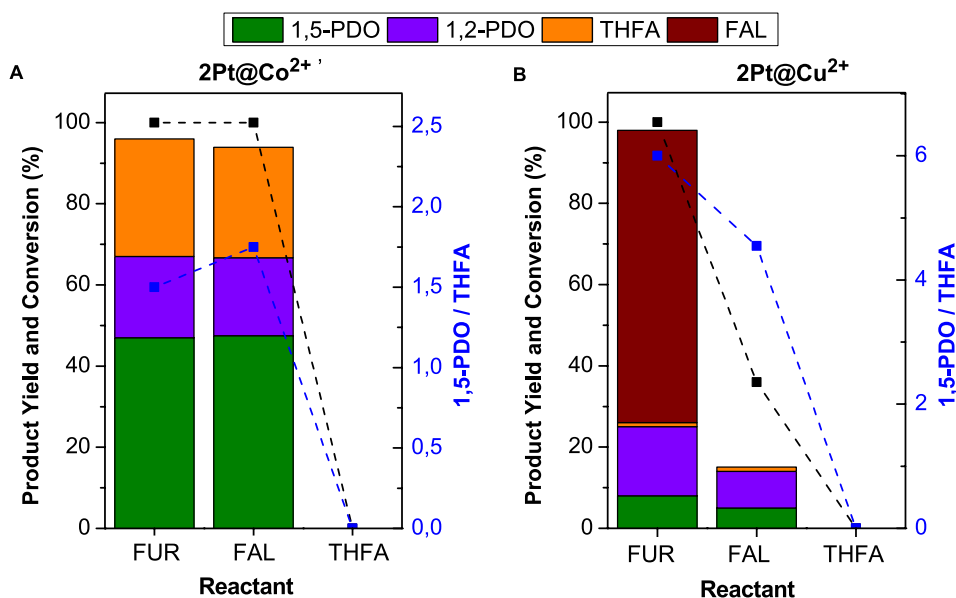

Fig. 4 Reaction pathways and side-reactions for the direct (via FAL) or indirect (via THFA) production of 1,5-PDO from FUR. 2-methylfuran (2-MF) is shown as possible side product

423 K are optimal for C−O hydrogenolysis into 1,5-PDO. Marked product yield differences are detected for $1Pt@Co^{2+}$, which can be especially attributed to the exponential increase of FAL conversion with temperature. Thus, these data indicate the relevance for keeping a balanced Pt content and temperature towards optimal 1,5-PDO productivity.

4 Conclusions

This letter shows the marked effects of bivalent metals and Pt within double layered hydrotalcite precursors on the direct formation of 1,5-pentanediol (1,5-PDO) from furfural. The present study concludes that Co^{2+} species outstand compared to other metals and that catalytic pathways proceed via the direct FAL conversion. Products yields are here optimized in terms of Pt content and catalysis temperature. These results contribute to understand the catalytic pathways and role of bivalent metals, leading to promising 1,5-PDO formation rates from furfural and the absence of the tetrahydrofurfuryl alcohol as reaction intermediate. Thus, the reported data and conditions aim to contribute towards the production of renewable diols relevant for the chemicals industry.

Fig. 5 FAL hydrogenation conversion and product yields (left axis) and 1,5-PDO/THFA molar ratio (right axis) for $xPt@Co^{2+}$ using 30 bar H_2 and 4 h of reaction as a function of Pt mass content and reaction temperature

Author Contributions AB: contributed to the experimental design and testing of catalysts and the writing of the manuscript. IG: contributed to the doctoral student supervision and manuscript revision. PLA:

References

1. Guan J, Peng G, Cao Q, Mu X (2014) Role of MoO_3 on a rhodium catalyst in the selective hydrogenolysis of biomass-derived tetrahydrofurfuryl alcohol into 1,5-pentanediol. J Phys Chem C 118(44):25555–25566. https://doi.org/10.1021/jp508313y

2. Huang K, Brentzel ZJ, Barnett KJ, Dumesic JA, Huber GW, Maravelias CT (2017) Conversion of furfural to 1,5-pentanediol: process synthesis and analysis. ACS Sustain Chem Eng 5(6):4699–4706. https://doi.org/10.1021/acssuschemeng.7b00059

3. Gavilà L, Lähde A, Jokiniemi J, Constanti M, Medina F, del Río E, Tichit D, Álvarez MG (2019) Insights on the one-pot formation of 1,5-pentanediol from furfural with Co−Al spinel-based nanoparticles as an alternative to noble metal catalysts. ChemCatChem 11(19):4944–4953. https://doi.org/10.1002/cctc.201901078

4. Xu W, Wang H, Liu X, Ren J, Wang Y, Lu G (2011) Direct catalytic conversion of furfural to 1,5-pentanediol by hydrogenolysis of the furan ring under mild conditions over Pt/Co_2AlO_4 catalyst. Chem Commun 47(13):3924–3926. https://doi.org/10.1039/c0cc05775d

5. Sulmonetti TP, Hu B, Lee S, Agrawal PK, Jones CW (2017) Reduced Cu–Co–Al mixed metal oxides for the ring-opening of furfuryl alcohol to produce renewable diols. ACS Sustain Chem Eng 5(10):8959–8969. https://doi.org/10.1021/acssuschemeng.7b01769

6. Wijaya HW, Kojima T, Hara T, Ichikuni N, Shimazu S (2017) Synthesis of 1,5-pentanediol by hydrogenolysis of furfuryl alcohol over Ni–Y_2O_3 composite catalyst. ChemCatChem 9(14):2869–2874. https://doi.org/10.1002/cctc.201700066

7. Gao F, Liu H, Hu X, Chen J, Huang Z, Xia C (2018) Selective hydrogenolysis of furfuryl alcohol to 1,5- and 1,2-pentanediol over Cu-$LaCoO_3$ catalysts with balanced Cu0-CoO sites. Cuihua Xuebao/Chin J Catal 39(10):1711–1723. https://doi.org/10.1016/S1872-2067(18)63110-9

8. Hernández WY, Lauwaert J, van der Voort P, Verberckmoes A (2017) Recent advances on the utilization of layered double hydroxides (LDHs) and related heterogeneous catalysts in a lignocellulosic-feedstock biorefinery scheme. Green Chem 19:5269–5302. https://doi.org/10.1039/c7gc02795h

9. Villaverde MM, Bertero NM, Garetto TF, Marchi AJ (2013) Selective liquid-phase hydrogenation of furfural to furfuryl alcohol over Cu-based catalysts. Catal Today 213:87–92. https://doi.org/10.1016/j.cattod.2013.02.031

10. Wang Y, Zhou M, Wang T, Xiao G (2015) Conversion of furfural to cyclopentanol on Cu/Zn/Al catalysts derived from hydrotalcite-like materials. Catal Lett 145(8):1557–1565. https://doi.org/10.1007/s10562-015-1539-y

11. Liu P, Derchi M, Hensen EJM (2014) Promotional effect of transition metal doping on the basicity and activity of calcined hydrotalcite catalysts for glycerol carbonate synthesis. Appl Catal B 144(1):135–143. https://doi.org/10.1016/j.apcatb.2013.07.010

12. Guo X, Zhang F, Evans DG, Duan X (2010) Layered double hydroxide films: synthesis, properties and applications. Chem Commun 46:5197–5210. https://doi.org/10.1039/c0cc00313a

13. Fu X, Ren X, Shen J, Jiang Y, Wang Y, Orooji Y, Xu W, Liang J (2021) Synergistic catalytic hydrogenation of furfural to 1,2-pentanediol and 1,5-pentanediol with LDO derived from CuMgAl hydrotalcite. Mol Catal 499:111298. https://doi.org/10.1016/j.mcat.2020.111298

14. Bruna L, Cardona-Farreny M, Colliere V, Philippot K, Axet MR (2022) In situ ruthenium catalyst modification for the conversion of furfural to 1,2-pentanediol. Nanomaterials 12(3):328. https://doi.org/10.3390/nano12030328

15. Chia M, Pagán-Torres YJ, Hibbitts D, Tan Q, Pham HN, Datye AK, Neurock M, Davis RJ, Dumesic JA (2011) Selective hydrogenolysis of polyols and cyclic ethers over bifunctional surface sites on rhodium–rhenium catalysts. J Am Chem Soc 133(32):12675–12689. https://doi.org/10.1021/ja2038358

16. Wijaya HW, Hara T, Ichikuni N, Shimazu S (2018) Hydrogenolysis of tetrahydrofurfuryl alcohol to 1,5-pentanediol over a nickel–yttrium oxide catalyst containing ruthenium. Chem Lett 47(1):103–106. https://doi.org/10.1246/cl.170920

17. Feng S, Nagao A, Aihara T, Miura H, Shishido T (2018) Selective hydrogenolysis of tetrahydrofurfuryl alcohol on $Pt/WO_3/ZrO_2$ catalysts: effect of WO_3 loading amount on activity. Catal Today 303:207–212. https://doi.org/10.1016/j.cattod.2017.08.058

18. Nakagawa Y, Tamura M, Tomishige K (2013) Catalytic reduction of biomass-derived furanic compounds with hydrogen. ACS Catal 3:2655–2668. https://doi.org/10.1021/cs400616p

19. Liu H, Huang Z, Kang H, Xia C, Chen J (2016) Selective hydrogenolysis of biomass-derived furfuryl alcohol into 1,2- and 1,5-pentanediol over highly dispersed Cu–Al_2O_3 catalysts. Cuihua Xuebao/Chin J Catal 37(5):700–710. https://doi.org/10.1016/S1872-2067(15)61080-4

20. Shao Y, Wang J, Sun K, Gao G, Li C, Zhang L, Zhang S, Xu L, Hu G, Hu X (2021) Selective hydrogenation of furfural and its derivative over bimetallic NiFe-based catalysts: understanding the synergy between Ni sites and Ni–Fe alloy. Renew Energy 170:1114–1128. https://doi.org/10.1016/j.renene.2021.02.056

21. Shao Y, Wang J, Du H, Sun K, Zhang Z, Zhang L, Li Q, Zhang S, Liu Q, Hu X (2020) Importance of magnesium in Cu-based catalysts for selective conversion of biomass-derived furan compounds to diols. ACS Sustain Chem Eng 8(13):5217–5228. https://doi.org/10.1021/acssuschemeng.9b07841

22. Pisal DS, Yadav GD (2019) Single-step hydrogenolysis of furfural to 1,2-pentanediol using a bifunctional Rh/OMS-2 catalyst. ACS Omega 4(1):1201–1214. https://doi.org/10.1021/acsomega.8b01595

23. Shao Y, Guo M, Wang J, Sun K, Zhang L, Zhang S, Hu G, Xu L, Yuan X, Hu X (2021) Selective conversion of furfural into diols over co-based catalysts: importance of the coordination of hydrogenation sites and basic sites. Ind Eng Chem Res 60(28):10393–10406. https://doi.org/10.1021/acs.iecr.1c01051

24. Pan Z, Wang R, Chen J (2018) Deoxygenation of methyl laurate as a model compound on Ni–Zn alloy and intermetallic compound catalysts: geometric and electronic effects of oxophilic Zn. Appl Catal B 224:88–100. https://doi.org/10.1016/j.apcatb.2017.10.040

25. Aristizábal A, Contreras S, Barrabés N, Llorca J, Tichit D, Medina F (2011) Catalytic reduction of nitrates in water on Pt promoted

Cu hydrotalcite-derived catalysts: effect of the Pt–Cu alloy formation. Appl Catal B 110:58–70. https://doi.org/10.1016/j.apcatb.2011.08.024

26. Kovanda F, Jiratova K, Rymes J, Kolousek D (2001) Characterization of activated CurMgrAl hydrotalcites and their catalytic activity in toluene combustion. Appl Clay Sci 18:71–80

27. Valente JS, Hernandez-Cortez J, Cantu MS, Ferrat G, López-Salinas E (2010) Calcined layered double hydroxides Mg–Me–Al (Me: Cu, Fe, Ni, Zn) as bifunctional catalysts. Catal Today 150(3–4):340–345. https://doi.org/10.1016/j.cattod.2009.08.020

28. Sitthisa S, Sooknoi T, Ma Y, Balbuena PB, Resasco DE (2011) Kinetics and mechanism of hydrogenation of furfural on Cu/SiO$_2$ catalysts. J Catal 277(1):1–13. https://doi.org/10.1016/j.jcat.2010.10.005

29. Xiong K, Wan W, Chen JG (2016) Reaction pathways of furfural, furfuryl alcohol and 2-methylfuran on Cu(111) and NiCu bimetallic surfaces. Surf Sci 652:91–97. https://doi.org/10.1016/j.susc.2016.02.011

30. Parikh J, Srivastava S, Jadeja GC (2019) Selective hydrogenation of furfural to tetrahydrofurfuryl alcohol using supported nickel–cobalt catalysts. Ind Eng Chem Res 58(35):16138–16152. https://doi.org/10.1021/acs.iecr.9b01443

31. Mizugaki T, Arundhathi R, Mitsudome T, Jitsukawa K, Kaneda K (2014) Highly efficient and selective transformations of glycerol using reusable heterogeneous catalysts. ACS Sustain Chem Eng 2(4):574–578. https://doi.org/10.1021/sc500006b

32. Taylor MJ, Jiang L, Reichert J, Papageorgiou AC, Beaumont SK, Wilson K, Lee AF, Barth JV, Kyriakou G (2017) Catalytic hydrogenation and hydrodeoxygenation of furfural over Pt(111): a model system for the rational design and operation of practical biomass conversion catalysts. J Phys Chem C 121(15):8490–8497. https://doi.org/10.1021/acs.jpcc.7b01744

33. Bus E, van Bokhoven JA (2007) Hydrogen chemisorption on supported platinum, gold, and platinum–gold–alloy catalysts. Phys Chem Chem Phys 9(22):2894–2902. https://doi.org/10.1039/b701402c

Publisher's Note Springer Nature remains neutral with regard to jurisdictional claims in published maps and institutional affiliations.

Authors and Affiliations

A. Barranca[1] · I. Gandarias[1] · P. L. Arias[1] · I. Agirrezabal-Telleria[1]

1   Department of Chemical and Environmental Engineering of the Bilbao Engineering School, University of Basque Country (UPV/EHU), Plaza Torres Quevedo 1, 48013 Bilbao, Spain